International Journal of Precision Engineering and Manufacturing (2022) 23:1–13
https://doi.org/10.1007/s12541-021-00591-1

Online ISSN 2005-4602
Print ISSN 2234-7593

REGULAR PAPER

A Novel Taper Design Method for Face-Milled Spiral Bevel and Hypoid Gears by Completing Process Method

Yu Yang[1,2] · Shimin Mao[3] · Wei Cao[1,2] · Yajun Huang[2]

Received: 13 November 2020 / Revised: 25 June 2021 / Accepted: 20 August 2021 / Published online: 29 October 2021
© Korean Society for Precision Engineering 2021

Abstract
For the face-milled spiral bevel and hypoid gears by the completing process method, in order to ensure that the tooth thickness and the tooth space width change in proportion to the cone distance, a novel taper design method is proposed. After the computation of blank dimensions of a gear pair according to ISO standard, the root angle of the wheel and the root angle of the pinion are redesigned based on the machining principle of the completing process method. Thus, the redesigned mean spiral angles of the wheel concave and convex tooth surface can be both equal to the original designed mean spiral angle of the wheel; likewise, the redesigned mean spiral angles of the pinion concave and convex tooth surface can be both equal to the original designed mean spiral angle of the pinion. By this, the ratios of the wheel tooth thickness and tooth space width to the wheel cone distance are more stable, and the ratios of the pinion tooth thickness and tooth space width to the pinion cone distance are more stable, too. Finally, this method is applied to a face-milled spiral hypoid gear pair, and the redesigned spiral angles of the wheel and the pinion are equal to the original designed mean spiral angles. For the wheel, the ranges of the ratios of the chordal thickness and the chordal space width to the cone distance are reduced more than 39% compared with those modified by ISO standard; for the pinion, the ranges of the ratios of the chordal thickness and the chordal space width to the cone distance are reduced more than 45% compared with those modified by ISO standard.

Keywords Taper design · Completing process method · Spiral bevel and hypoid gear · Blank modification · Spiral angle

1 Introduction

Gears are essential transmission components in many areas such as aviation, automobile, engineering machinery, and so on [1–3]. In recent years, for face-milled spiral bevel and hypoid gears, the completing process method is widely used for increased efficiency, cost reduction, machining accuracy improvement, and tooth strength enhancement. The "completing process method" is an advanced manufacturing method, also named the "duplex helical method", "duplex spread-blade method" and "double-cut method". It includes only two processes: (a) finish machining of the wheel and (b) finish machining of the pinion. Compared with the traditional "five-cut method", the "completing process method" is characterized by only one cutter for machining both the concave and convex flank of the pinion simultaneously [4–6].

For the standard-depth-taper face-milled gear pair, the tooth space width and the tooth thickness width change in proportion to the cone distance at any particular section along the face width. As Fig. 1 shows, the spiral angle β_{mV} at the concave mean point P_V along the pitch cone and the spiral angle β_{mX} at the convex mean point P_X along the pitch cone are equal, and they are both equal to the designed mean spiral angle. Now the concave tooth line and the convex tooth line tilt to each other [7]. But with the completing process method, the cutter cuts the concave flank and the convex flank simultaneously. Assuming that the concave tooth line mm stays the same, then the convex tooth line turns into $n'n'$ from nn. If by the formate method, the concave tooth line mm and the convex tooth line $n'n'$ are approximately two concentric circular arcs, and do not tilt to each other any

✉ Yu Yang
yangyu@chd.edu.cn

1 Key Laboratory of Road Construction Technology and Equipment, Ministry of Education, Chang'an University, Xi'an 710064, China

2 Shantui Construction Machinery Co., Ltd., Jining 272073, China

3 State Key Laboratory for Manufacturing Systems Engineering, Xi'an Jiaotong University, Xi'an 710049, China

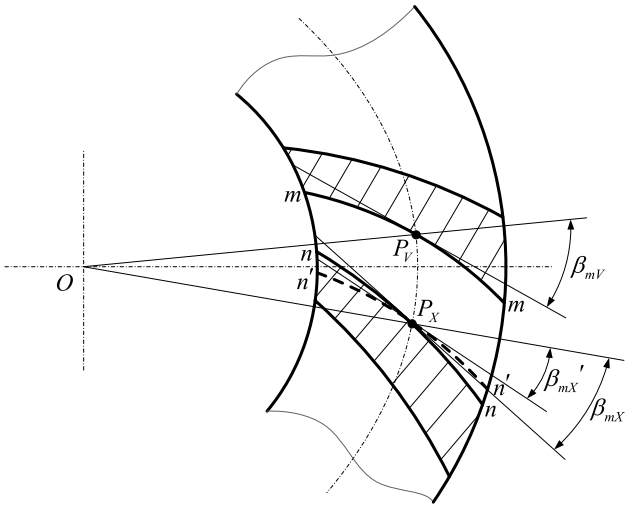

Fig. 1 Pitch plane of face-milled spiral bevel gear

more [8]. Therefore, the completing process method leads to less material removed from the heel and more material removed from the toe, resulting in thicker tooth thickness width at the heel and thinner tooth thickness width at the toe than normal. In essence, the spiral angle β_{mV} and β_{mX} become unequal, so the tooth space width and the tooth thickness width cannot shrink in proportion to the cone distance, which affects proper meshing of gear pair. Hence, the gear blank dimensions need to be redesigned. Since the values of the cutter diameter, the pressure angle and the spiral angle are determined, the root angle is the only parameter that can be modified.

The Gleason Company proposed the completing process method in the 1930s and disclosed the calculating instructions for the generated small face-milled spiral bevel gears duplex helical method (SGDH) in 1965 [9]. The improved method was applicable to large-module face-milled spiral bevel gears up to 1978 [10]. But the manufacturing principles are not publicly disclosed.

In recent years, scholars have continued research into the completing process method. Shtipelman pointed out that when both gear and pinion were generated by the duplex method, the gear and pinion dedendum angles had to be computed so that the spiral angles at the opposite sides of the gear and pinion teeth would have initial values, respectively [11]. In [7], the abnormal contraction of the tooth thickness width and tooth space width caused by the duplex helical method was introduced, and the formulas of the duplex taper were derived. In [8], the duplex contraction of the exact duplex helical method by the Gleason Works was introduced, and the calculating formula of the sum of the root angle of the gear and pinion was deduced, and the sum was distributed according to tooth depth ratio of inclined point. In [12], the basic machine settings of the spiral bevel and hypoid gears generated by the duplex helical method were determined, and the hypoid gear dimensions were modified based on the root angle of the pinion. In [13], three reference points were used to calculate the basic machine-tool settings for spiral bevel and hypoid gears manufactured by the duplex helical method, and the resulting new mean dedendum of the pinion was different from the mean dedendum of the hypoid gears' blank dimensions, and the modified mean dedendum was used. For the completing process method, some other studies were also carried out, such as meshing performance analysis [14], tooth surface reconstructing method [15], tooth surface modification [16], and flank deviation correction [17]. These studies lay a foundation for the development of the completing process method. But the machining principle of the completing process method is not taken into account in the existing gear blank modification method.

This paper proposes a novel taper design method for face-milled spiral bevel and hypoid gears by the completing process method based on the machining principle. The root angles of the wheel and the pinion are redesigned after the computation of blank dimensions of a gear pair according to ISO standard. The wheel is cut by the formate method, an appropriate root angle of the wheel is searched by iteration so that the spiral angle β_{mWV} at the wheel concave mean point and β_{mWX} at the wheel convex mean point along the pitch cone are both equal to the original designed wheel mean spiral angle. The pinion is cut by the generating method, and in the same way, an appropriate root angle of the pinion is searched by iteration so that the spiral angle β_{mPV} at the pinion concave mean point and β_{mPX} at the pinion convex mean point along the pitch cone are both equal to the original designed pinion mean spiral angle. In this way, the ratios of the wheel tooth thickness and tooth space width to the wheel cone distance are more stable, and the ratios of the pinion tooth thickness and tooth space width to the pinion cone distance are more stable, too.

In order to ensure that the change of the whole tooth depth along the face width is relatively even, the root line is tilted about the root mean point. Thus, the mean addendum and the mean dedendum stay the same before and after the redesign.

The goal is blank modification for the completing process method, and the machine-tool settings in this paper are calculated based on the conventional primary cradle-type generator. Gear blank design is the first step of gear development. After the step of blank modification, the machining principle of the completing process method will be studied, and it will be based on the CNC free-form type generator. Then, the machine-tool settings of the completing process method on the CNC free-form type generator will be determined based on the contact characteristics [18] for good performance. The method is applicable to face-milled spiral bevel and hypoid gear by the completing process

method. After redesign by this method, a duplex taper will be developed.

2 Redesign of Wheel Root Angle

The original design of the blank dimensions is accomplished according to ISO standard [19]. The redesign process of the wheel root angle is as follows.

2.1 Determination of Wheel Cutter Parameters

The wheel can be cut by the formate method or by the generating method [20]. Since the wheel is usually cut by the formate method to increase efficiency in actual production [21] when the pitch angle is larger than 70°, the wheel is cut by the formate method here. If this method is to be applied to the wheel by the generating method, then the formulas in Sect. 2.2 and Sect. 2.3 are replaced by the formulas of the generating method.

The inner blade angle and the outer blade angle of the wheel cutter are equal to the pressure angle at the concave root mean point and the pressure angle at the convex root mean point, respectively. The inner blade angle of the wheel cutter is positive, and the outer blade angle is negative. The cutter radius of the wheel r_{cW} is selected from standard specifications. The point width of the wheel cutter can be determined by the following equations.

If the backlash is not considered, the tooth space width of the wheel should be equal to the tooth thickness width of the pinion [22]. Figure 2 is the pitch plane of the wheel. The outer circular tooth thickness of the wheel S_{eW} and the outer circular tooth thickness of pinion S_{eP} are already determined during the original computation of blank dimensions. The mean circular tooth space width of the wheel cd can be calculated as follows:

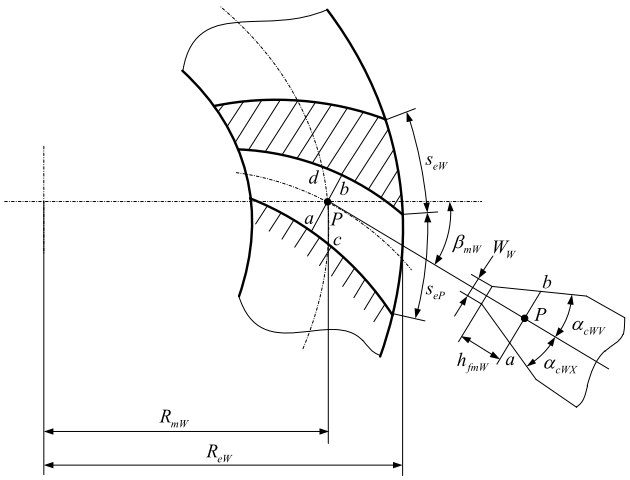

Fig. 2 Point width of wheel cutter

$$cd \approx \frac{R_{mW}}{R_{eW}} S_{eP} \tag{1}$$

where R_{mW} is the mean cone distance of the wheel, and R_{eW} is the outer cone distance of the wheel.

The mean pitch normal chordal tooth space width of the wheel $\overline{ab}$ can be obtained by the following equation:

$$\overline{ab} = cd \cos \beta_{mW} \tag{2}$$

where β_{mW} is the mean spiral angle of the wheel.

The point width of the wheel cutter can be determined as follows:

$$W_W = \overline{ab} - h_{fmW}\left(\tan \alpha_{cWX} + \tan \alpha_{cWV}\right) \tag{3}$$

where h_{fmW} is the mean dedendum of the wheel, and can be calculated by the original designed parameters because it does not change.

2.2 Determination of Wheel Machine Settings

Since the blade angles of the wheel cutter are equal to the corresponding pressure angle at the root mean point, the axis of the wheel cutter is perpendicular to the root cone of the wheel, which means that there is no tilt angle [23]. The wheel machine settings (shown in Fig. 3) can be determined as follows:

Vertical:

$$V_W = r_{cW} \cos \beta_{mRW} \tag{4}$$

Horizontal:

$$H_W = L_{mW} - r_{cW} \sin \beta_{mRW} \tag{5}$$

where $L_{mW} = R_{mW} \cos\left(\delta_W - \delta_{fW}\right) + \left(t_{zRW} - t_{zW}\right) \cos \delta_{fW}$.

Cradle angle:

$$q_W = \arctan\left(\frac{V_W}{H_W}\right) \tag{6}$$

Radial distance:

$$s_W = \sqrt{V_W^2 + H_W^2} \tag{7}$$

Machine root angle:

$$\Gamma_{MW} = \delta_{fW} \tag{8}$$

Machine center to crossing point:

$$\Delta X_W = t_{zRW} \tag{9}$$

where δ_{fW} is the root angle of the wheel, t_{zRW} is the root apex beyond crossing point of the wheel, t_{zW} is the pitch apex beyond crossing point of the wheel.

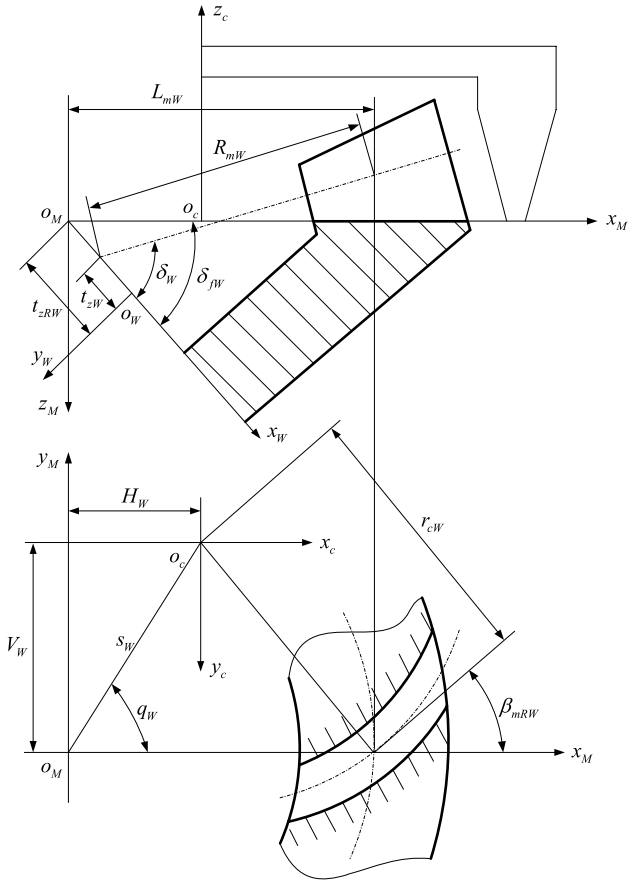

Fig. 3 Wheel machining principle

2.3 Calculation of Wheel Mean Point Parameters

With the formate method, the tooth surface of the wheel is a complete copy of the conical surface of the wheel cutter [24]. Any point on the cutter surface can be expressed by a set of parameters (h_c, θ_c), and h_c represents the height from the cutter top plane to this point along the cutter axis, and θ_c represents the rotation angle in the cutter transverse plane. With the coordinate of the wheel pitch mean point on the rotation projection plane given, the corresponding parameters (h_c, θ_c) on the cutter surface can be obtained by iteration, with which the position vector r_c and the normal vector n_c of this point in the cutter coordinate system can be expressed. Then the position vector r_W and the normal vector n_W of the wheel pitch mean point in the wheel coordinate system can be obtained through coordinate transformation. The position vector and the normal vector of the wheel concave mean point P_{WV} and convex mean point P_{WX} can be calculated by the following equations.

$$r_W = M_{WM} M_{Mc} r_c \tag{10}$$

$$n_W = m_{WM} m_{Mc} n_c \tag{11}$$

Here, the transfer matrix from the cutter coordinate system to the machine coordinate system is:

$$M_{Mc} = \begin{bmatrix} 1 & 0 & 0 & H_W \\ 0 & -1 & 0 & V_W \\ 0 & 0 & -1 & 0 \\ 0 & 0 & 0 & 1 \end{bmatrix} \tag{12}$$

$$m_{Mc} = \begin{bmatrix} 1 & 0 & 0 \\ 0 & -1 & 0 \\ 0 & 0 & -1 \end{bmatrix} \tag{13}$$

The transfer matrix from the machine coordinate system to the wheel coordinate system:

$$M_{WM} = \begin{bmatrix} \cos\Gamma_{MW} & 0 & -\sin\Gamma_{MW} & -\Delta X_W \\ -\sin\Gamma_{MW} & 0 & \cos\Gamma_{MW} & 0 \\ 0 & -1 & 0 & 0 \\ 0 & 0 & 0 & 1 \end{bmatrix} \tag{14}$$

$$m_{WM} = \begin{bmatrix} \cos\Gamma_{MW} & 0 & -\sin\Gamma_{MW} \\ -\sin\Gamma_{MW} & 0 & \cos\Gamma_{MW} \\ 0 & -1 & 0 \end{bmatrix} \tag{15}$$

2.4 Calculation of Spiral Angle

With the position vector and the normal vector of a point on a gear tooth flank given, the spiral angle at this point along the pitch tooth line can be obtained. As Fig. 4 shows, x is the gear axis, and θ is the directed angle in yz plane, which can be determined by the following piecewise function.

$$\begin{cases} y > 0, z > 0: \ \theta = \arctan(z/y) \\ y > 0, z < 0: \ \theta = \arctan(z/y) + 2\pi \\ y < 0: \ \theta = \arctan(z/y) + \pi \\ y = 0, z > 0: \ \theta = \pi/2 \\ y = 0, z < 0: \ \theta = 3\pi/2 \\ y > 0, z = 0: \ \theta = 0 \\ y < 0, z = 0: \ \theta = -\pi \end{cases} \tag{16}$$

In the axial section plane xr, N is the unit normal vector at that point perpendicular to the pitch cone, pointing to the outside of the pitch cone. L is the normal vector along the pitch cone generatrix, pointing to the gear heel. T is the unit tangent vector at that point along the pitch tooth line. These vectors can be obtained as follows:

$$N = \left\{ -\sin\delta \ \ \cos\delta\cos\theta \ \ \cos\delta\sin\theta \right\} \tag{17}$$

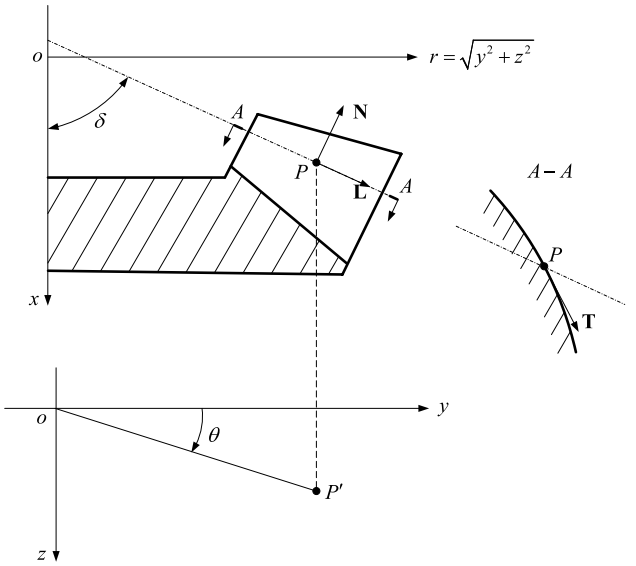

Fig. 4 Spiral angle at any point

$$T = N \times n / |N \times n| \tag{18}$$

$$L = \left\{ \cos\delta \;\; \sin\delta\cos\theta \;\; \sin\delta\sin\theta \right\} \tag{19}$$

where n is the calculated normal vector at this point, and δ is the pitch angle.

Then the spiral angle at this point along the pitch cone can be obtained by this:

$$\beta = a\cos(L \cdot T) \tag{20}$$

If the calculated $\beta > \pi/2$, then $\beta = \pi - \beta$.

The spiral angle β_{mWV} at the wheel concave mean point and β_{mWX} at the wheel convex mean point along the pitch line can be determined by the above method.

This method can be applied to any type of bevel gear, if δ is replaced by other cone angle, then the calculated spiral angle is along that cone angle.

2.5 Redesign of Wheel Root Angle

The demand for the wheel blank by the completing process method is: the redesigned wheel concave mean spiral angle β_{mWV} and the redesigned wheel convex mean spiral angle β_{mWX} along the pitch cone are equal, and both equal to the original designed mean spiral angle β_{mW}. The constrain can be expressed by the following equation:

$$\beta_{mWX} = \beta_{mWV} = \beta_{mW} \tag{21}$$

This equation is equivalent to two independent constrains. When the two independent variables, that is the wheel root angle δ_{fW} and the wheel root mean spiral angle β_{mRW}, are assigned new values, the wheel machine settings are recalculated, then new β_{mWV} and β_{mWX} are obtained. Through iteration like this, the appropriate new wheel root angle δ'_{fW} and new wheel root mean spiral angle β'_{mRW} can be searched finally. The iteration is based on the secant method.

During iteration, the initial value of the wheel root angle can be given the original designed parameter, and the initial value of the wheel root mean spiral angle can be calculated by the original designed parameters.

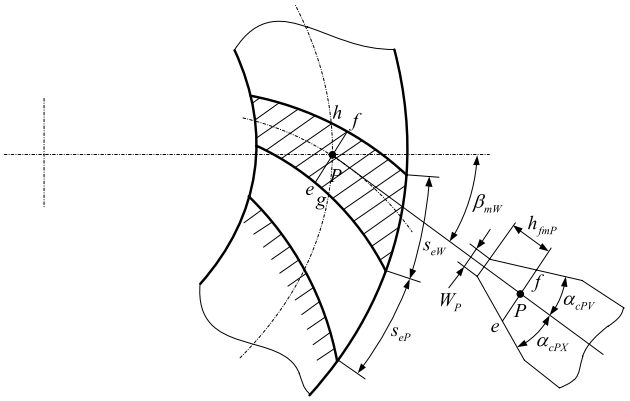

Fig. 5 Point width of pinion cutter

3 Redesign of Pinion Root Angle

3.1 Determination of Pinion Cutter Parameters

The cutter radius of the pinion r_{cP} is selected from standard specifications.

The inner blade angle α_{cPX} and the outer blade angle α_{cPV} of the pinion cutter are equal to the pinion convex and concave mean root pressure angle, respectively. The inner blade angle is negative, and the outer blade angle is positive.

After the wheel root angle is redesigned, the coordinate of the redesigned wheel concave mean point and the redesigned wheel convex mean point are determined. But these two points are two endpoints of the mean tooth space circular arc of the wheel. Then the convex mean point is turned an angular pitch about the wheel axis so that these two points become two endpoints of the wheel mean tooth thickness circular arc. Thus, the circular tooth thickness gh (shown in Fig. 5) can be determined.

The mean normal chordal tooth thickness of the wheel can be calculated as follows:

$$\overline{ef} \approx gh\cos\beta_{mW} \tag{22}$$

If the backlash is not taken into account, the pinion tooth space width should be equal to the wheel tooth thickness

width at the pitch plane. The pinion cutter pitch width *ef* should be equal to the pinion mean normal chordal tooth space width. So the point width of the pinion cutter can be estimated by the following equation.

$$W_P = \overline{ef} - h_{fmP}\left(\tan\left|\alpha_{cPX}\right| + \tan\left|\alpha_{cPV}\right|\right) \tag{23}$$

where h_{fmP} is the pinion mean dedendum.

3.2 Determination of Pinion Machine Settings

The axis of the pinion cutter is perpendicular to the pinion root cone, so there is no tilt. The pinion machine settings (shown in Fig. 6) can be determined as follows:

Vertical:

$$V_P = r_{cP}\cos\beta_{mRP} \tag{24}$$

Horizontal:

$$H_P = L_{mP} - r_{cP}\sin\beta_{mRP} \tag{25}$$

where $L_{mP} = R_{mP}\cos\left(\delta_P - \delta_{fP}\right)$.

Cradle angle:

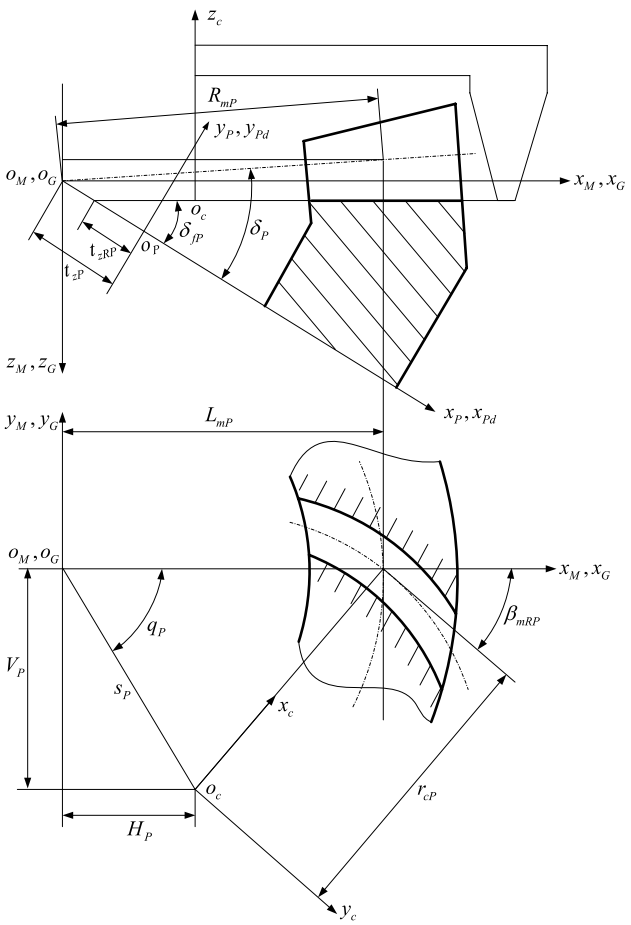

Fig. 6 Machining principle of pinion

$$q_P = \arctan\left(\frac{V_P}{H_P}\right) \tag{26}$$

Radial distance:

$$s_P = \sqrt{V_P^2 + H_P^2} \tag{27}$$

Roll ratio:

$$R_{aP} = \frac{L_{mP}}{R_{mP}\sin\delta_P} \tag{28}$$

Machine root angle:

$$\Gamma_{MP} = \delta_{fP} \tag{29}$$

Here, β_{mRP} is the pinion mean root spiral angle, and R_{mP} is the pinion mean cone distance, and δ_P is the pinion pitch angle, and δ_{fP} is the pinion root angle.

3.3 Calculation of Pinion Mean Point Parameters

The pinion is cut by the generating method, and the cradle rotates with the cutter on it, which can be imaged as a generating gear that meshes with the pinion with line contact at the roll ratio. Any point on the cutter surface can be expressed with a set of $\left(h_c, \theta_c\right)$. As the same with the wheel, h_c represents the height along the cutter axis from the cutter top plane to this point, and θ_c represents the directed angle on the cutter transverse plane. When the coordinate of the pinion mean point on the rotation projection plane is given, the corresponding parameters $\left(h_c, \theta_c\right)$ on the cutter surface can be solved by iteration. The rotation angle of the generating gear can be determined through meshing equation. The position vector r_c and the normal vector n_c of this point on the cutter in the cutter coordinate system can be expressed in the pinion coordinate system by transfer matrix, and becomes the position vector $\mathbf{r}_P$ and the normal vector n_P on the pinion flank, which can be calculated as follows:

$$r_P = M_{PPd}M_{PdM}M_{MG}M_{Gc}r_c \tag{30}$$

$$n_P = m_{PPd}m_{PdM}m_{MG}m_{Gc}r_c \tag{31}$$

Here, the transfer matrix from the cutter coordinate system to the generating gear coordinate system is:

$$M_{Gc} = \begin{bmatrix} \sin\beta_{mRP} & \cos\beta_{mRP} & 0 & s_P\cos q_P \\ \cos\beta_{mRP} & -\sin\beta_{mRP} & 0 & -s_P\sin q_P \\ 0 & 0 & -1 & \left(t_{zP} - t_{zRP}\right)\sin\delta_{fP} \\ 0 & 0 & 0 & 1 \end{bmatrix} \tag{32}$$

$$m_{Gc} = \begin{bmatrix} \sin\beta_{mRP} & \cos\beta_{mRP} & 0 \\ \cos\beta_{mRP} & -\sin\beta_{mRP} & 0 \\ 0 & 0 & -1 \end{bmatrix} \tag{33}$$

The transfer matrix from the generating gear coordinate system to the machine coordinate system is:

$$M_{MG} = \begin{bmatrix} \cos\varphi_{GP} & -\sin\varphi_{GP} & 0 & 0 \\ \sin\varphi_{GP} & \cos\varphi_{GP} & 0 & 0 \\ 0 & 0 & 1 & 0 \\ 0 & 0 & 0 & 1 \end{bmatrix} \tag{34}$$

$$m_{MG} = \begin{bmatrix} \cos\varphi_{GP} & -\sin\varphi_{GP} & 0 \\ \sin\varphi_{GP} & \cos\varphi_{GP} & 0 \\ 0 & 0 & 1 \end{bmatrix} \tag{35}$$

where φ_{GP} represents the rotation angle of the generating gear about the axis z_G, and its value is positive if the rotation direction is in accord with the right-hand rule, otherwise negative.

The transfer matrix from the machine coordinate system to the fixed pinion coordinate system is:

$$M_{PdM} = \begin{bmatrix} \cos\delta_{fP} & 0 & \sin\delta_{fP} & -t_{zP} \\ \sin\delta_{fP} & 0 & -\cos\delta_{fP} & 0 \\ 0 & 1 & 0 & 0 \\ 0 & 0 & 0 & 1 \end{bmatrix} \tag{36}$$

$$m_{PdM} = \begin{bmatrix} \cos\delta_{fP} & 0 & \sin\delta_{fP} \\ \sin\delta_{fP} & 0 & -\cos\delta_{fP} \\ 0 & 1 & 0 \end{bmatrix} \tag{37}$$

The transfer matrix from the fixed pinion coordinate system to the moving pinion coordinate system is:

$$M_{PPd} = \begin{bmatrix} 1 & 0 & 0 & 0 \\ 0 & \cos\varphi_P & \sin\varphi_P & 0 \\ 0 & -\sin\varphi_P & \cos\varphi_P & 0 \\ 0 & 0 & 0 & 1 \end{bmatrix} \tag{38}$$

$$m_{PPd} = \begin{bmatrix} 1 & 0 & 0 \\ 0 & \cos\varphi_P & \sin\varphi_P \\ 0 & -\sin\varphi_P & \cos\varphi_P \end{bmatrix} \tag{39}$$

where φ_P represents the rotation angle of the pinion about the axis x_P, and its value is positive if the rotation direction is in accord with the right-hand rule, otherwise negative.

In the machining process of the pinion, the generating gear and the pinion accord with meshing equation [25], through which the rotation angle of the generating gear φ_{GP} and that of the pinion φ_P can be obtained.

The meshing equation can be simplified as follows:

$$U\sin\varphi_{GP} + V\cos\varphi_{GP} = W \tag{40}$$

Then the rotation angle of the generating gear can be calculated using the following equation:

$$\tan\frac{\varphi_{GP}}{2} = \frac{U - \sqrt{U^2 + V^2 - W^2}}{W + V} \tag{41}$$

Then the rotation angle of the pinion:

$$\varphi_P = R_{aP} \cdot \varphi_{GP} \tag{42}$$

where

$$\begin{cases} U = T_y\cos\delta_{fP} \\ V = -T_x\cos\delta_{fP} \\ W = -T_z\left(1/R_{aP} - \sin\delta_{fP}\right) \end{cases} \tag{43}$$

$$\begin{cases} T_x = y_G^G nz_G^G - z_G^G ny_G^G \\ T_y = z_G^G nx_G^G - x_G^G nz_G^G \\ T_z = c_G^G ny_G^G - y_G^G nx_G^G \end{cases} \tag{44}$$

$\left(x_G^G, y_G^G, z_G^G\right)$ is the position vector in the generating gear coordinate system that r_c is turned into by the transfer matrix M_{MG} and M_{Gc}, and $\left(nx_G^G, ny_G^G, nz_G^G\right)$ is the normal vector in the generating gear coordinate system that n_c is turned into by the transfer matrix m_{MG} and m_{Gc}.

3.4 Redesign of Pinion Root Angle

With the coordinate on the rotation projection plane given, the position vectors and the normal vectors of the pinion concave mean point and the pinion convex mean point can be obtained by the above equations. According to the calculation method of the spiral angle in Sect. 2.4, the pinion concave mean spiral angle β_{mPV} and the pinion convex mean spiral angle β_{mPX} along the pinion pitch line can be calculated.

The demand for the pinion blank by the completing process method is: the redesigned spiral angle β_{mPV} and β_{mPX} are both equal to the original designed pinion mean spiral angle β_{mP}, which can be expressed as:

$$\beta_{mPX} = \beta_{mPV} = \beta_{mP} \tag{45}$$

This equation contains two independent constrains. When the pinion root angle δ_{fP} and the pinion root mean spiral angle β_{mRP} are changed, the pinion machine settings are recalculated as well as the spiral angle β_{mPV} and β_{mPX}. This iteration is executed till the above constrain is satisfied, then the redesigned pinion root angle δ'_{fP} and the redesigned pinion root mean spiral angle β'_{mRP} are finally determined. The iteration is based on the secant method.

During the iteration, the initial value of the pinion root angle can be given the original designed value, and the initial value of pinion root mean spiral angle can be calculated with the original designed parameters.

4 Redesign of Other Relevant Blank Dimensions

With the redesigned wheel root angle δ'_{fW} determined, the face cone of the pinion needs to be parallel to the root cone of the wheel; in the same way, with the redesigned pinion root angle δ'_{fP} determined, the face cone of the wheel needs to be parallel to the root cone of the pinion. Then the wheel face angle and the pinion face angle are redesigned as follows:

$$\begin{cases} \delta'_{aP} = \Sigma - \delta'_{fW} \\ \delta'_{aW} = \Sigma - \delta'_{fP} \end{cases} \tag{46}$$

where δ'_{aP} is the redesigned pinion face angle, and δ'_{aW} is the redesigned wheel face angle, and Σ is the shaft angle.

With the mean addendum and dedendum of the gear pair staying the same, after the wheel root angle and the pinion root angle are redesigned, some other relevant blank dimensions change subsequently. The following equations apply to both the wheel and the pinion.

(1) The unchanged mean addendum h_{am} and dedendum h_{fm} :

$$\begin{cases} h_{am} = h_{ae} - \dfrac{b}{2}\tan\left(\delta_a - \delta\right) \\ h_{fm} = h_{fe} - \dfrac{b}{2}\tan\left(\delta - \delta_f\right) \end{cases} \tag{47}$$

where b represents face width, and h_{ae} represents outer addendum, and h_{fe} represents outer dedendum, and δ_a represents face angle, and δ represents pitch angle, and δ_f represents root angle, and the values of these parameters before redesign are used.

(2) After the redesigned root angle δ'_f is determined, the corresponding changed parameters are:

Dedendum angle:

$$\theta'_f = \delta - \delta'_f \tag{48}$$

Outer dedendum:

$$h'_{fe} = h_{fm} + \frac{b}{2}\tan\theta'_f \tag{49}$$

Inner dedendum:

$$h'_{fi} = h_{fm} - \frac{b}{2}\tan\theta'_f \tag{50}$$

Root apex beyond crossing point:

$$t'_{zR} = t_z + \left(R_e\sin\delta - h'_{fe}\cos\delta\right)/\tan\delta'_f - R_e\cos\delta - h'_{fe}\sin\delta \tag{51}$$

(3) After the redesigned face angle δ'_a is determined, the corresponding changed parameters are:

Addendum angle:

$$\theta'_a = \delta'_a - \delta \tag{52}$$

Outer addendum:

$$h'_{ae} = h_{am} + \frac{b}{2}\tan\theta'_a \tag{53}$$

Inner addendum:

$$h'_{ai} = h_{am} - \frac{b}{2}\tan\theta'_a \tag{54}$$

Face apex beyond crossing point:

$$t'_{zF} = t_z + \left(R_e\sin\delta + h'_{ae}\cos\delta\right)/\tan\delta'_a + h'_{ae}\sin\delta - R_e\cos\delta \tag{55}$$

Outer diameter:

$$d'_{ae} = d_e + 2h'_{ae}\cos\delta \tag{56}$$

Crown to crossing point:

$$t'_{xo} = \frac{d'_{ae}}{2\tan\delta'_a} - t'_{zF} \tag{57}$$

Front crown to crossing point:

$$t'_{xi} = t'_{xo} - b\frac{\cos\delta'_a}{\cos\theta'_a} \tag{58}$$

Here, the symbol "′" means the redesigned value, and if without this symbol, it means using the original designed value.

5 Numerical Examples and Discussion

A spiral hypoid gear pair is redesigned by this new method after blank design of standard depth taper according to ISO standard. And the results are compared with those of the duplex taper modified by ISO standard. The basic parameters of this gear pair is shown in Table 1.

Through iteration, the redesigned wheel concave mean spiral angle β_{mWV} and the redesigned convex mean spiral angle β_{mWX} are both equated to the original designed wheel

Table 1 Basic parameters of gear pair

	Pinion	Wheel
Offset (mm)	26	
Shaft angle (°)	90	
Spiral hand	Left	Right
Number of teeth	7	39
Mean spiral angle (°)	43.85	35.836
Average pressure angle (°)	22.5	
Pitch angle (°)	11.889	77.997
Outer cone distance (mm)	211.297	217.301
Method	Generating	Formate

mean spiral angle. The original designed wheel mean spiral angle β_{mW} is 35.836°, and the redesigned wheel root angle by iteration δ'_{fW} is 75.3628°, and the redesigned wheel root mean spiral angle β'_{mRW} is 35.9427°. The wheel mean point parameters are compared between redesign by the new method and modification by ISO standard in Tables 2 and 3.

After the redesign of the wheel, the point width of the pinion cutter is estimated at 4.709 mm. Through iteration, the redesigned pinion concave and convex mean spiral angle are both equated to the original designed pinion mean spiral angle. The original designed pinion mean spiral angle is 43.850000°, and the redesigned pinion root angle δ_{fP} is 10.9948°, the redesigned pinion root mean spiral angle β_{mRP} is 43.8498°. The pinion mean point parameters are compared between redesign by the new method and modification by ISO standard in Tables 4 and 5. It can be observed that for the duplex taper modified by ISO standard, the wheel concave and convex mean spiral angle are not equal to the original designed wheel mean spiral angle; and after redesign by the new method, the wheel concave and the convex mean spiral angle are both equal to the original designed wheel mean spiral angle. Likewise, both the pinion concave and convex mean spiral angle become equal to the original designed pinion mean spiral angle after redesign, though they are not for the duplex taper modified by ISO standard.

After the wheel and pinion root angle are redesigned, the other relevant blank dimensions are changed as Table 6 shows.

The wheel chordal thicknesses and chordal space widths along the wheel pitch cone are shown in Table 7. The pinion chordal thicknesses and chordal space widths along the pinion pitch cone are shown in Table 8.

The ratios of the wheel chordal thickness to the wheel cone distance at a series of sections along the wheel pitch cone are plotted in Fig. 7a. For the duplex taper modified by ISO standard, the range of the ratios of the wheel chordal

Table 2 Comparison of parameters of wheel concave mean point

Parameter	Modified by ISO standard	Redesigned by new method
Position vector (mm)	(36.8527, − 182.4101, − 10.5846)	(36.8527, − 182.5949, − 6.6752)
Normal vector	(− 0.4775, 0.4847, − 0.7329)	(− 0.4697, 0.4848, − 0.7378)
Pitch mean spiral angle (°)	34.955313	35.836014

Table 3 Comparison of parameters of wheel convex mean point

Parameter	Modified by ISO standard	Redesigned by new method
Position vector (mm)	(36.8527, − 182.7131, − 1.1863)	(36.8527, − 182.6991, 2.5513)
Normal vector	(0.2486, 0.6085, − 0.7536)	(0.2597, 0.5982, − 0.7581)
Pitch mean spiral angle (°)	35.415733	35.836015

Table 4 Comparison of parameters of pinion concave mean point

Parameter	Modified by ISO standard	Redesigned by new method
Position vector (mm)	(181.0077, 36.5858, 4.5474)	(181.0077, 36.5859, 4.5465)
Normal vector	(− 0.7052, 0.3409, − 0.6217)	(− 0.7031, 0.3464, − 0.6210)
Pitch mean spiral angle (°)	43.994136	43.849999

Table 5 Comparison of parameters of pinion convex mean point

Parameter	Modified by ISO standard	Redesigned by new method
Position vector (mm)	(181.0077, 36.6076, − 4.3690)	(181.0077, 36.6077, − 4.3682)
Normal vector	(− 0.5550, − 0.5651, − 0.6104)	− 0.5588, − 0.5607, − 0.6110)
Pitch mean spiral angle (°)	43.723408	43.849999

thickness is from 0.047143 to 0.050981; and for the redesign by the new method, the range is from 0.047149 to 0.049451. The ratios of the wheel chordal space width to the wheel cone distance are plotted in Fig. 7b. For the duplex taper modified by ISO standard, the range of the ratios of the wheel chordal space width is from 0.106546 to 0.110378; and for the redesign by the new method, the range is from 0.108073 to 0.110373. The range of the ratios of the wheel chordal thickness to the wheel cone distance is reduced 40.02% after redesign by the new method, and it means that the ratios of the wheel chordal thickness to the wheel cone distance are more stable after redesign. Likewise, the range of the ratios of the wheel chordal space width to the wheel cone distance is reduced 39.98% after redesign by the new method, and it means that the ratios of wheel chordal space width to the wheel cone distance are more stable after redesign, too.

The ratios of the pinion chordal thickness to the pinion cone distance at a series of sections along the pinion pitch cone are plotted in Fig. 8a. For the duplex taper modified by ISO standard, the range of the ratio of the pinion chordal thickness is from 0.129003 to 0.132872; and for the redesign by the new method, the range is from 0.130454 to 0.132581. The ratios of the pinion chordal space width to the pinion cone distance are plotted in Fig. 8b. For the duplex taper modified by ISO standard, the range of the ratio of the pinion chordal space width is from 0.04951 to 0.053559; and for the redesign by the new method, the range is from 0.049816 to 0.052042. The range of the ratios of the pinion chordal thickness to the pinion cone distance is reduced 45.02% after redesign by the new method, and it means that the ratios of the pinion chordal thickness to the pinion cone distance are more stable after redesign. Likewise, the range of the ratios of the pinion chordal space width to the pinion cone distance

Table 6 Comparison of parameters of gear pair

Parameter	Wheel		Pinion	
	Modified by ISO standard	Redesigned by new method	Modified by ISO standard	Redesigned by new method
Root angle (°)	74.647	75.3628	11.448	10.9948
Dedendum angle (°)	3.350	2.6342	0.441	0.8942
Outer dedendum (mm)	15.565	15.1823	3.561	3.8163
Inner dedendum (mm)	11.994	12.3758	3.063	2.8067
Root apex beyond crossing point (mm)	− 0.949	− 3.3578	− 15.643	− 8.6108
Face angle (°)	78.442	79.0052	15.210	14.6372
Addendum angle (°)	0.445	1.0082	3.321	2.7482
Outer addendum (mm)	1.840	2.1398	13.947	13.6226
Inner addendum (mm)	1.366	1.0664	3.561	10.5175
Face apex beyond crossing point (mm)	2.151	0.2795	0.509	7.8617
Outer diameter (mm)	425.865	425.9900	114.357	113.7221
Crown to crossing point (mm)	41.395	41.1025	209.784	209.8509
Front crown to crossing point (mm)	29.173	29.4668	147.258	147.1912

Table 7 Comparison of wheel chordal thickness and chordal space width along pitch cone

Section	Wheel cone distance (mm)	Wheel chordal thickness (mm)		Wheel chordal space width (mm)	
		Modified by ISO standard	Redesigned by new method	Modified by ISO standard	Redesigned by new method
0	156.301	7.926982	7.36942	16.69452	17.25139
1	162.401	8.270612	7.79873	17.31183	17.78315
2	168.501	8.590324	8.20081	17.95304	18.34209
3	174.601	8.885875	8.57511	18.61839	18.92878
4	180.701	9.156964	8.920962	19.30816	19.54388
5	186.801	9.403221	9.237552	20.02274	20.18821
6	192.901	9.624209	9.523915	20.76256	20.86273
7	199.001	9.819423	9.778896	21.52812	21.56859
8	205.101	9.988286	10.00113	22.31999	22.30717
9	211.201	10.130155	10.18897	23.13882	23.08008
10	217.301	10.244324	10.3405	23.98531	23.88926

Table 8 Comparison of pinion chordal thickness and chordal space width along pitch cone

Section	Pinion cone distance (mm)	Pinion chordal thickness (mm)		Pinion chordal space width (mm)	
		Modified by ISO standard	Redesigned by new method	Modified by ISO standard	Redesigned by new method
0	146.61	18.91307	19.16842	7.852272	7.585412
1	153.0787	19.90849	20.11614	8.030604	7.813369
2	159.5474	20.88921	21.04792	8.224117	8.057948
3	166.0161	21.85355	21.9618	8.434661	8.321243
4	172.4848	22.79939	22.85539	8.664486	8.605787
5	178.9535	23.72416	23.72576	8.916345	8.914665
6	185.4222	24.62466	24.56931	9.193629	9.251671
7	191.8909	25.49688	25.38151	9.500565	9.621517
8	198.3596	26.33574	26.1567	9.842485	10.03014
9	204.8283	27.13471	26.88756	10.22622	10.48512
10	211.297	27.88526	27.56457	10.66068	10.99635

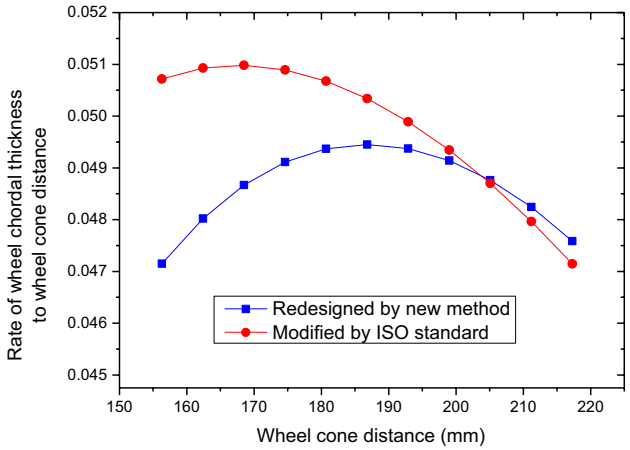

(a) The ratio of the wheel chordal thickness

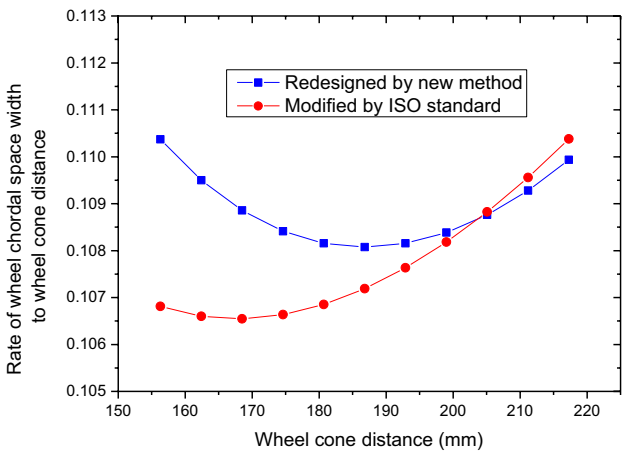

(b) The ratio of the wheel chordal space width

Fig. 7 The ratio of the wheel chordal thickness and chordal space width to the wheel cone distance. **a** The ratio of the wheel chordal thickness. **b** The ratio of the wheel chordal space width

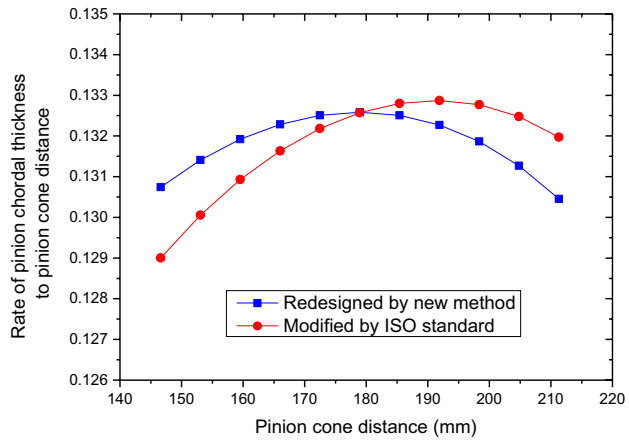

(a) The ratio of the pinion chordal thickness

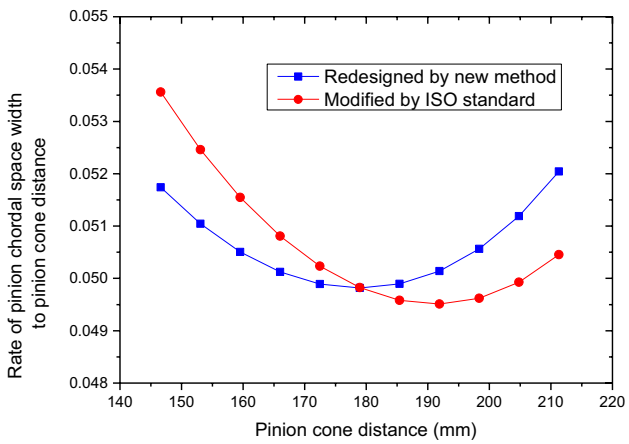

(b) The ratio of the pinion chordal space width

Fig. 8 The ratio of the pinion chordal thickness and chordal space width to the pinion cone distance. **a** The ratio of the pinion chordal thickness. **b** The ratio of the pinion chordal space width

is reduced 45.02% after redesign by the new method, and it means that the ratios of the pinion chordal space width to the pinon cone distance are more stable after redesign, too.

The gear pair in this paper is with offset, this method also applies to face-milled spiral bevel gear pair without offset.

6 Conclusion

This paper proposes an novel calculation method of taper design based on machining theory aiming at spiral bevel and hypoid gears by the completing process method. With which, for both the wheel and the pinion, the redesigned concave and convex mean spiral angle can be both equal to its respective original designed mean spiral angle. Thus, the ratios of the wheel tooth thickness and tooth space width to the wheel cone distance are more stable, and the ratios of the pinion tooth thickness and tooth space width to the pinion cone distance are more stable, too. Finally, this method is applied to a spiral hypoid gear pair, and it can be drawn that for the wheel, the ranges of the ratios of the chordal thickness and the chordal space width to the cone distance are reduced more than 39% compared with those modified by ISO standard; for the pinion, the ranges of the ratios of the chordal thickness and the chordal space width to the cone distance are reduced more than 45% compared with those modified by ISO standard.

Acknowledgements This work was supported by National Natural Science Foundation of China (Grant No. 51805405) and the Fundamental Research Funds for the Central Universities (Grant No. 300102251102).

References

1. Chen, B., Liang, D., & Li, Z. (2014). A study on geometry design of spiral bevel gears based on conjugate curves. *International Journal of Precision Engineering and Manufacturing, 15*(3), 477–482.
2. Mertens, A. J., & Senthilvelan, S. (2016). Durability of polymer gear-paired with steel gear manufactured by wire cut electric discharge machining and hobbing. *International Journal of Precision Engineering and Manufacturing, 17*(2), 181–188.
3. Tian, X. Q., Han, J., Xia, L. (2015). Precision control and compensation of helical gear hobbing via electronic gearbox Cross-Coupling controller. International Journal of Precision Engineering & Manufacturing.
4. Kawasaki, K., & Tamura, H. (1997). Method for cutting hypoid gears (duplex spread-blade method). *Jsme International Journal, 400*, 4644–4650.
5. Kawasaki, K., & Tamura, H. (1998). Duplex spread blade method for cutting hypoid gears with modified tooth surface. *Journal of Mechanical Design, 120*, 441–447.
6. Pisula, J., & Płocica, M. (2011). Numerical model of bevel gears cutting by duplex helical method. *Key Engineering Materials., 490*, 237–246.
7. Zeng, T. (1989). Design and manufacture of spiral bevel gears. Harbin Technical University Press.
8. Wang, Z., Liu, Q., Zhang, D. (1995). The exact duplex helical method in generation of spirial bevel gears(I)—The blank design of the spirial bevel gears. Journal of Jilin Forestry University 11.
9. The Gleason Works. (1985). Generated spiral bevel gears duplex helical method including grinding (SGDH). Rochester.
10. The Gleason Works. (1978). Electronic computer program Aoo212
11. Shtipelman, B. A. (1978). Design and manufacture of hypoid gears.
12. Zhang, Y., Yan, H. Z., & Zeng, T. (2015). Cutting principle and tooth contact analysis of spiral bevel and hypoid gears generated by duplex helical method. *Journal of Mechanical Engineering, 51*, 15–23.
13. Zhang, Y., Yan, H. Z., & Zeng, T. (2015). Computerised design and simulation of meshing and contact of formate hypoid gears generated with a duplex helical method. *Journal of Mechanical Engineering, 61*, 523–532.
14. Pisula, J. (2016). An analysis of the effect of the application of helical motion and assembly errors on the meshing of a spiral bevel gear using duplex helical method. *Advances in Manufacturing Science and Technology., 40*, 19–31.
15. Deng, C., Yan, H. Z., Chen, Y. Z., & Yi, W. B. (2019). Tooth surface reconstructing method of spiral bevel gear generated by duplex helical method based on renewal Kriging model. *Journal of Central South University (Science and Technology), 50*, 1351–1356.
16. Yan, H. Z., Wu, S. X., & Xiao, M. (2019). Effect of tooth surface zoning modification by duplex helical method on reducing sensitivity of installation error. *Journal of Central South University (Science and Technology), 50*, 286–294.
17. Geng, L. L., Deng, J., Nie, S. W., Deng, X. Z., Jiang, C., & Han, Z. Y. (2020). Research on mathematical model and flank deviation correction of spiral bevel gear by duplex helical method. *Journal of Mechanical Transmission, 44*, 7–13.
18. Mu, Y. M., Li, W. L., Fang, Z. D., & Zhang, X. J. (2018). A novel tooth surface modification method for spiral bevel gears with higher-order transmission error. *Mechanism and Machine Theory, 126*, 49–60.
19. ISO 23509: Bevel and hypoid gear geometry (2006).
20. Wang, P. Y., & Fong, Z. H. (2005). Adjustability improvement of face-milling spiral bevel gears by modified radial motion (MRM) method. *Mechanism & Machine Theory, 40*(1), 69–89.
21. Litvin, F. L., Fuentes, A., Fan, Q., & Handschuh, R. F. (2002). Computerized design, simulation of meshing, and contact and stress analysis of face-milled formate generated spiral bevel gears. *Mechanism and Machine Theory, 37*, 441–459.
22. Wu, X. T. (1979). Machining principle and machine settings of tilted formate generated spiral bevel gears. Xi'an Jiaotong University Scientific and Technical Report.
23. Wu, X. T. (1981). Machine settings of tilted formate generated spiral bevel and hypoid gears. Machine tool, vol 11.
24. Litvin, F. L., & Fuentes, A. (2004). *Gear geometry and applied theory* (2nd ed.). Cambridge University Press.
25. Guo, Z., Mao, S. M., Li, X. E., Ren, Z. Y. (2016). Research on the theoretical tooth profile errors of gears machined by skiving. Mechanism and machine theory, vol 97, (pp. 1–11).

Publisher's Note Springer Nature remains neutral with regard to jurisdictional claims in published maps and institutional affiliations.

Yu Yang received her Ph.D. degree in mechanical engineering from Xi'an Jiaotong University, China. She is currently a engineer at School of Construction Machinery, Chang'an University, China. Her research interests include gear transmission theory and technology.

Wei Cao received his Ph.D. degree in mechanical engineering from Sichuan University, Chengdu, China, in 2019. Now, he is a lecturer at School of Construction Machinery, Chang'an University. His research interests are tribology, dynamics, and fatigue in transmission systems.

Shimin Mao is a professor of mechanical engineering at Xi'an Jiaotong University, China. He received his Ph.D. degree from Xi'an Jiaotong University, China, in 1989. His research interests include high precision CNC machining and quality control of complex curved surface, CNC machining technology and equipment of precision large gear.

Yajun Huang is the director of Research Institute of Shantui Construction Machinery Co.,Ltd., China. He received his master's degree from Shandong University, China, in 2015. His research interests include construction machinery technology.